HHS Public Access

Author manuscript

Toxicol Ind Health. Author manuscript; available in PMC 2020 December 22.

Published in final edited form as:

Toxicol Ind Health. 2020 April ; 36(4): 250–262. doi:10.1177/0748233720921683.

In vitro toxicity assessment of respirable solid surface composite sawing particles

W Kyle Mandler[1], **Seungkoo Kang**[2], **Mariana Farcas**[1], **Chaolong Qi**[2], **Sherri A Friend**[1], **Yong Qian**[1]

[1]Health Effects Laboratory Division, National Institute for Occupational Safety and Health, Morgantown, WV, USA

[2]Division of Field Studies and Engineering, National Institute for Occupational Safety and Health, Cincinnati, OH, USA

Abstract

Solid surface composites (SSCs) are a class of popular construction materials composed of aluminum trihydrate and acrylic polymers. Previous investigations have demonstrated that sawing SSC releases substantial airborne dusts, with a number-based geometric mean diameter of 1.05 μm. We reported that in mice, aspiration exposure to airborne SSC dusts induced symptoms of pulmonary inflammation at 24-h postexposure: neutrophilic influx, alveolitis, and increased lactate dehydrogenase (LDH) and pro-inflammatory cytokine levels in lavage fluid. The particles appeared to be poorly cleared, with 81% remaining at 14-day postexposure. The objective of this study was to determine the toxicity specifically of respirable particles on a model of human alveolar macrophages (THP-1). The relative toxicities of subfractions (0.07, 0.66, 1.58, 5.0, and 13.42 μm diameter) of the airborne particles were also determined. THP-1 macrophages were exposed for 24 h to respirable particles from sawing SSC (0, 12.5, 25, 50, or 100 μg/ml) or size-specific fractions (100 μg/ml). Exposure to respirable SSC particles induced THP-1 macrophage toxicity in a dose-dependent manner. Viability was decreased by 15% and 19% after exposure to 50 and 100 μg/ml SSC, respectively, which correlated with increased cell culture supernatant LDH activity by 40% and 70% when compared to control. Reactive oxygen species (ROS) production and inflammatory cytokines were increased in a dose-dependent manner. A size-dependent cytotoxic effect was observed in the cells exposed to subfractions of SSC particles. SSC particles of 0.07, 0.66, and 1.58 μm diameter killed 36%, 17%, and 22% of cells, respectively. These results indicate a potential for cytotoxicity of respirable SSC particles and a relationship between particle size and toxicity, with the smallest fractions appearing to exhibit the greatest toxicity.

Corresponding author: Yong Qian, Health Effects Laboratory Division, National Institute for Occupational Safety and Health, 1095 Willowdale Road, Morgantown, WV 26505, USA. yaq2@cdc.gov.

Declaration of conflicting interests

The author(s) declared no potential conflicts of interest with respect to the research, authorship, and/or publication of this article.

Keywords

In vitro; aluminum hydroxide; nanoparticle; occupational health; macrophage; size dependency; dose dependency

Introduction

Solid surface composites (SSCs), most commonly associated with the Corian® brand, are a widely produced class of building material with a variety of applications. Frequently used in the construction of countertops and sink basins, but also furniture, building cladding, and a variety of other applications (DuPont, 2018), SSC can be sawed, sanded, thermo-formed, and extruded into almost any shape. A recent countertop study by The Freedonia Group (Freedonia, 2015) forecasted an annual growth of 4.2% through 2019 in the US countertop industry. Among the forecasted US$29B countertop market in 2019, SSC countertops are estimated to have a market share of 13.0% (increased from 12.4% in 2009). Thus, the size of the workforce manufacturing SSC materials and performing fabrication and installation of SSC countertops is expected to grow from a conservative estimate of 18,000 workers in the United States in 2012, based on the market share data and the published estimate of the workforce in stone countertop fabrication (Phillips and Johnson, 2012).

The composition of SSC materials varies depending on the manufacturer and application, but the principal components include aluminum trihydrate (ATH, aluminum hydroxide), acrylic polymers, and other proprietary binders and colorants. Depending on the application, SSC may contain other materials with known pulmonary hazards, including silica, asbestos (Fugazzi, 1998), and quartz (Simmons, 2004). During the fabricating processes of SSC, such as sanding and sawing, high concentrations of particles and volatile organic chemicals (VOCs) can be produced (Kang et al., 2019). Exposure to these emissions could pose a health hazard to workers. In addition, manufacturing and fabricating products containing plastic (acrylate polymers) is known to release ultrafine particles (diameters < 100 nm) and VOCs (Unwin et al., 2013).

Raghu et al. (2014a, 2014b) reported on the case of a worker who was exposed to SSC dusts for 16 years in a home workshop. This worker developed pulmonary interstitial fibrosis that ultimately proved fatal, with ATH and aluminum oxide detected in the lung at autopsy. The manufacturer of Corian® responded to these findings by noting that the aluminum present in the biopsies could come from sources other than the SSC materials, such as the aluminum oxide in sandpaper, and that other workspace contaminants could have also contributed to the observed pathologies (Gannon and Rickard, 2014; McKeever et al., 2014). Thus, a controlled study of the toxicity of exposure to SSC particles alone is of considerable importance to ensure worker and consumer safety. In our previous investigation of the in vivo toxicity of SSC (Mandler et al., 2019), dust was limited in one important regard: The particle population delivered via aspiration in that case contained many large particles, which would not ordinarily be respirable by a mouse or even a human. Thus, it is possible that some of the observed toxicity in that study may be due to the presence of these particles and not the smaller, respirable fraction. The objective of the current study is to establish and

characterize the ability of purely respirable size fractions of SSC to elicit cytotoxicity in an alveolar macrophage model.

Our group has characterized the particles released by SSC sawing (Qi et al., 2016). That study utilized an automated tool-testing chamber wherein 1.2-cm thick SSC boards were cut using a circular saw and dust samples were measured in real-time and collected on filters for characterization. The particles measured in real-time showed a number-based geometric mean aerodynamic diameter of 1.05 μm with a geometric standard deviation of 1.78 and another substantial peak for ultrafine particles at 11.8 nm in mobility diameter. The airborne SSC dusts collected on the polyvinyl chloride (PVC) filter samples have an estimated ATH content of 86.0 ± 6.6%. In a more recent study examining respirable size fractions of SSC sawing dust, the respirable dust generation rate obtained using a micro-orifice uniform deposit impactor (MOUDI) was 5.9 mg/g of total dust, suggesting that 0.59% of the mass removed by sawing SSC becomes respirable dust (Kang et al., 2019). ATH content was greater than 85% in most fractions in the respirable size range. VOC analysis indicated that methyl methacrylate (MMA) was the most abundant compound released at a rate of 69 μg/g. In a subsequent in vivo study (Mandler et al., 2019), we exposed male C57BL/6 mice to SSC dusts suspended in saline via a single oropharyngeal aspiration at a range of doses from 25 μg to 1 mg. At days 1 and 14 postexposure, lungs were collected and fixed for histopathologic analysis. We observed that a single exposure to SSC sawing dust (collected using the previously described automatic sawing apparatus) induced pro-inflammatory changes in the murine lung. Following oropharyngeal aspiration of SSC dust, dose-dependent alveolar inflammation and granulomatous mass formation were observed across all exposure levels. The particles appeared to be poorly cleared, with 81% of the original lung burden still present at day 14. We also observed increased levels of lactate dehydrogenase (LDH), polymorphonuclear leukocytes (PMN), eosinophils, and macrophages in the bronchoalveolar lavage fluid (BALF) collected from exposed animals. We detected elevated levels of various pro-inflammatory and pro-fibrotic cytokines compared to controls in the BALF, including interleukin 1 beta (IL-1β), tumor necrosis factor alpha (TNFα), and interferon gamma (IFNγ). While this study only observed animals for a short time period (14 days) following a single exposure, the findings are indicative of a substantial hazard posed by exposure to SSC dusts. The mechanisms behind the observed toxicity have yet to be elucidated.

Methods

SSC particle generation and collection

As previously described by Qi et al. (2016), in this study, we mounted a Makita circular saw (Model 5057KB, Makita USA, Inc., La Mirada, California, USA) in the chamber and operated it automatically. A 60-tooth, 18.4 cm diameter Triple Chip Grind saw blade specifically designed for aluminum cutting (Model 072560, Oshlun, Inc., Henderson, Nevada, USA) was used for the saw. The traverse speed of the saw cutting through the Corian® board was set at 0.635 cm/s.

We collected respirable dust samples on polytetrafluoroethylene (PTFE) filters (47 mm diameter, 5 μm pore size) in conductive filter cassettes with a GK4.162 RASCAL cyclone

sampler (Mesa Laboratories, Inc., Lakewood, Colorado, USA) at a flow rate of 9.0 l/min. We also collected size-classified airborne dust samples from a sampling port on the duct using a high-flow micro-orifice uniform deposit impactor (HF-MOUDI 131, TSI, Inc., Shoreview, Minnesota, USA). The HF-MOUDI was equipped with PTFE filters (75 mm diameter) as substrates for collecting dust samples on five size stages with a flow rate of 100 l/min. The mass of the collected dust on each stage was obtained by pre-weighing and post-weighing the PTFE filter. The sampling probe connecting the HF-MOUDI and the duct provided isokinetic sampling at the operating flow rate. Following collection, the filters were weighed and placed in 50 ml conical tubes containing 40 ml ultra-pure sterile water. The filters were sonicated for 1 min using a Branson 450 ultrasonicator (Emerson Industrial Automation, St. Louis, Missouri, USA) to release the particles into suspension. After drying, the filters were post-weighted to determine the amount of material collected in suspension. The recovery rate (based on comparison with particle collection weights) was 90–95%.

Particle size distribution

The morphology and size of SSC particles were determined using field emission scanning electron microscopy (FE-SEM). A 0.1% (weight/weight (w/w)) suspension of particles using saline was prepared and sonicated for 3 min (energy delivered = 1000 J). The final concentration was 0.02% (w/w) and 1 ml was passed through a 0.2-μm polycarbonate filter (Steriltech Corp., Kent, Washington, USA). A section from each filter was imaged at 2 K magnification using 5 kV accelerating voltage (Hitachi S-4800, Hitachi High Technologies America, Inc., Dallas, Texas, USA). Ten fields of view were randomly chosen for imaging, capturing a total of 361 particles, the diameters of which were measured using ImageJ software (National Institutes of Health, Bethesda, Maryland, USA).

Endotoxin detection

While particle generation and collection were carried out in sterile laboratory environments, potential endotoxin contamination could provide false-positive cytotoxicity, ROS, and cytokine results. Endotoxin was measured using Pierce™ LAL Chromogenic Endotoxin Quantitation Kit (Thermo Scientific, Waltham, Massachusetts, USA). According to the manufacturer's instructions, a standard curve was generated using the provided endotoxin as a standard. The level of endotoxin for all samples was below the detection limit of 0.05 EU/ml.

Cell culture

TSP-1 cells (human acute monocytic leukemia cell line), purchased from American Type Culture Collection, were grown in Roswell Park Memorial Institute (RPMI) 1640 medium (Invitrogen, Carlsbad, California, USA) supplemented with 10% fetal bovine serum and 1% penicillin/streptomycin. Cells were plated onto 96-well plates at 2×10^4 cells/well in 200 μl of RPMI 1640 media. Cells were transformed into a macrophage-like phenotype by 24-h incubation in RPMI media with 60 ng/ml phorbol 12-myristate 13-acetate. Prior to exposure, the cells were incubated in clear, serum-free RPMI 1640 media for 6 h. All exposures were carried out in clear, serum-free RPMI 1640 media. Exposure concentrations were 12.5, 25, 50, and 100 μg/ml SSC for 24 h. Following exposure, 20 μl of cell culture supernatant was

used for LDH analysis, and the remainder was reserved and frozen at −80°C for later analysis.

Transmission electron microscopy

After THP-1 were exposed to respirable SSC dust at 100 μg/ml for 24h, the cells were trypsinized and centrifuged at 1500 × *g* for 5 min at room temperature and then fixed with Karnovsky's fixative (2.5% glutaraldehyde, 2.5% paraformaldehyde in 0.1 M sodium cacodylic buffer). The samples were postfixed in osmium tetroxide, mordanted in 1% tannic acid and stained en bloc in 0.5% uranyl acetate, embedded in epon, sectioned, and stained with 4% uranyl acetate and Reynold's lead citrate. Sections were imaged with the JEOL 1400 transmission electron microscope (Tokyo, Japan).

Cytotoxicity assays

Cell culture supernatant LDH activity, a measure of cell membrane integrity and particle cytotoxicity, was measured using an LDH (liquid) reagent set (Pointe Scientific, Canton, Michigan, USA) according to manufacturer's instructions. Briefly, 20 μl of culture supernatant was added to 200 μl reagent in a pre-warmed 96-well plate. After 5 min of incubation at 37°C, absorbance at 340 nm was read. Following a subsequent 60-s incubation, the plate was read again at the same wavelength.

Following the collection of supernatants from 96-well plates, cells were washed with 100 μl/well of clear RPMI 1640 media, after which 200 μl/well of clear RPMI with 10% Alamar blue dye was added. The Alamar blue reagent, resazurin, acts as an indicator of cell health and metabolic function by being reduced by components of the electron transport chain into highly fluorescent resorufin in a linear manner relative to the number of living cells. The cells were incubated for 2 h at 37°C in the Alamar solution. Following incubation, the plates were read at an excitation of 560 nm and emission of 590 nm.

ROS stress assays

A 100 μl of clear RPMI with 200 nM chloromethyl dichlorodihydrofluorescein diacetate (CM-H_2DCFDA) (Invitrogen, C6827) was added to 100 μl of existing media and cells. CM-H_2DCFDA is capable of passively translocating into the cytosol, where ROS cleavage and oxidation generate a fluorescent adduct. Fluorescence from 8 wells to 12 wells for each exposure concentration was measured in a fluorescence microplate reader at an excitation of 485 nm and emission wavelength 535 nm.

To measure glutathione peroxidase (GPx) activity, 40 μl of the reaction mixture was added to each well (Abcam, ab102530). The plate was incubated at room temperature for 15 min. The plate was read at 340 nm, and immediately afterward 10 μl of cumene hydroperoxide solution was added to each sample, positive control and reagent control wells only. Output was measured on a microplate reader at 340 nm. Following a subsequent incubation at 25°C for 5 min, the plate was read again at 340 nm.

Pro-inflammatory cytokines

V-Plex Human Proinflammatory Panel 1 Human cytokine kits (K15049D-1) were purchased from Mesoscale Discovery (Rockville, Maryland, USA). Assay diluent (25 µl) was added to all wells and the plate was sealed and incubated for 30 s at room temperature on an orbital shaker (600 r/min). THP-1 cell culture supernatant, standards, and controls were added at 25 µl per well. The plate was sealed and incubated for 2 h at room temperature on an orbital shaker (600 r/min). At the end of the incubation, the wells were washed three times using 200 µl phosphate-buffered saline + 0.05% Tween 20, soaked for 30 s, and then discarded. Detection antibody was added at 25 µl per well, and the plate was sealed and incubated for 1 h at room temperature on an orbital shaker (600 r/min). At the end of the incubation, the plate was washed three times. MSD Read Buffer (150 µl) was added to each well and the MSD plates were measured on the MSD Sector Imager 2400 plate reader.

SSC size-classified aluminum content

Size-classified samples were analyzed for elemental aluminum using a modified NIOSH Method 7303 (NIOSH, 2003) for using PVC filters with its detection limit determined by the blank filters (0.3 µg). The samples were collected by a MOUDI with 12 stages (Model 110, TSI Inc.) and the results were reported in the previous publication (Kang et al., 2019). In this article, we interpolated the aluminum content (based on the ratio of the molecular mass of elemental aluminum compared to ATH) obtained from the 12 particle sizes in MOUDI into the 5 particle sizes in HI-MOUDI.

Statistical analysis

A D'Agostino and Pearson omnibus normality test was used to assess the homogeneity of variance. In cases where non-normal data sets were detected, statistical comparisons were made with Kruskal-Wallis tests and post hoc Dunn's multiple comparisons test for between-subject effects where appropriate. For normally distributed data sets, a one-way analysis of variance was performed to compare the main effects for each variable. When significant main effects were observed, a Holms-Sidak post hoc test was used to determine where significant differences existed between the groups. Technical replicates were conducted in triplicate, $n = 3–4$ for each experiment. In all cases, $p < .05$ was used to establish statistical significance. In the case of size-fraction cytotoxicity, a linear regression was performed to confirm a size-dependent effect. All data are reported as mean ± standard error of mean (SEM), unless otherwise noted.

Results

Respirable particle characterization and macrophage interactions

In our previous investigation, mice were exposed to particles with a number-based geometric mean diameter of 1.16 µm (Mandler et al. 2019). However, a substantial portion of the mass of these particles was composed of larger, non-respirable particles. In this study, using specifically collected respirable particles, the geometric mean particle size (from FE-SEM) (depicted in Figure 1) was 0.72 µm, with a geometric standard deviation of 2.9. There appeared to be little or no particle aggregation in the captured images, indicating effective

dispersion. Overall, 95.6% of the observed particles were smaller than 4 μm in diameter. Transmission electron microscopy (TEM) analysis revealed that some particles appear to be capable of crossing the plasma membrane and localizing in the cytoplasm (Figure 2(a)), while others were observed contained in phagolysosomes (Figure 2(b)).

Respirable SSC exposure induces macrophage cytotoxicity

Particle cytotoxicity can be detected as a decrease in cellular metabolic activity. The resazurin in Alamar blue is taken into the cell, where the reducing potential of mitochondrial activity converts it to the highly fluorescent resorufin in a linear rate proportional to the number of living cells. A decreased rate of this conversion is indicative of decreased cell metabolism and viability (Figure 3). In this study, SSC exposure reduced viability by 15.2 ± 4.8% at 50 μg/ml and 19.0 ± 3.9% at 100 μg/ml. Particle-cell interactions often result in membrane disruption and necrosis, allowing LDH to leak into the cell culture medium. SSC cell culture supernatant LDH activity was increased by 48.5 ± 9.9% at 25 μg/ml, 40.0 ± 10.4% at 50 μg/ml, and 70.7 ± 10.2% at 100 μg/ml.

ROS are often detected as a by-product of both macrophage lysosomal activity and as a marker of necrosis. CM-H_2DCFDA is cell permeant but is cleaved by intracellular esterases and retained thereafter in the cytosol. Oxidation by ROS yields fluorescent dichloroflourescein, which can be detected fluoroscopically. As measured by CM-H_2DCFDA fluorescence (Figure 4), ROS were increased by 63.6 ± 6.6% at the 50 μg/ml level and 105.8 ± 7.5% at 100 μg/ml. GPx activity was increased by 21.7 ± 2.7%, 17.3 ± 2.0%, and 19.4 ± 2.6% at the 12.5, 25, and 50 μg/ml exposure levels, respectively.

Respirable SSC exposure induces inflammatory cytokine secretion

In response to the presence of foreign material, alveolar macrophages become activated and release increased quantities of cytokines, chemokines, and growth factors. Pro-inflammatory cytokines in the THP-1 cell culture supernatant were measured via multiplex assay (Figure 5). IL-4 was increased in response to all doses. IL-1β and IL2, IL10, IFNγ, and IL-12p70 were increased at 6.25 μg/ml and above doses. TNFα was increased at 12.5 μg/ml and above exposure levels, while IL-13 was only increased slightly at 25 and 100 μg/ml exposures. IL-6 levels remained unchanged at all doses.

SSC size-fraction cytotoxicity

To determine the relative toxicity among various size fractions of SSC dust, THP-1 macrophages were exposed to equal mass concentrations of 0.07, 0.66, 1.58, 5.0, or 13.5 μm diameter particles for 24 h. THP-1 cell culture supernatant LDH activity was measured following exposure (Figure 6). Supernatant from wells containing cells incubated for 5 min with Triton X-100 0.01% (volume/volume) was used as a measure of total LDH content. At 100 μg/ml, 0.07, 0.66, and 1.58 μm particles induced the release of 36%, 18%, and 22% of total LDH, respectively. A simple linear regression was performed to confirm size-dependency, resulting in a finding of significant ($p = 0.04$) non-zero slope ($F = 4.669$, degrees of freedom numerator, degrees of freedom demominator = 1, 18).

SSC size-fraction aluminum content

It is possible that the varying composition of the size fractions could account for some of the observed toxicity differential. The elemental aluminum content (Table 1) of 13.5, 5, 1.58, 0.66, and 0.07 μm diameter SSC particles was 19%, 27%, 30%, 37%, and 24%, respectively. By using the molecular formula for ATH, we can estimate the relative ATH content of the particles for each size fraction. In this case, we calculated that the ATH content of 13.5, 5, 1.58, 0.66, and 0.07 μm diameter SSC particles was 52%, 74%, 83%, 102%, and 66%, respectively.

Discussion

Our group has previously established that sawing SSC generates a large quantity of airborne dust, much of which is respirable. We also recently demonstrated that pulmonary exposure to airborne SSC dust in mice resulted in pulmonary inflammation. However, because the particle population in that study was a mixture of all the emitted airborne dust generated by sawing and thus contained many large (>5 μm diameter) particles, some of the observed toxicity may have been the result of particles that would not normally be respirable. To determine if purely respirable-sized SSC particles are capable of eliciting toxicity, we exposed human THP-1 derived macrophages to several size fractions of specifically respirable SSC particles across a wide dose range.

Several factors likely contribute to SSC particle toxicity, of which the most important is particle size distribution. For most particles, toxicity is negatively correlated with particle size, and smaller particles tend to generate a greater cytotoxic response per unit mass (Oberdörster, 2000). This size-dependent toxicity is an attribute possibly owed to a combination of size-dependent factors, including deposition characteristics, high surface area to mass, and surface chemistries unique to the nanoscale. As determined by FE-SEM, 5.8% of the respirable SSC particles were nano-sized (diameter <100 nm) and 35.4% were 0.66 μm or smaller. Particles in this size range tend to have a much higher rate of alveolar deposition (Geiser and Kreyling, 2010) and are preferentially taken up by alveolar macrophages (AM) (Hardy et al., 2013; Wagner et al., 2007), compared to larger particles. Nano aluminum oxide is more toxic than micron-sized (Stanley et al., 2010). Thus, a heterogeneous mixture of particles with a large fraction of nanoparticles may be more bioactive than another mixture without. This principle was largely supported by our findings. However, some interesting differences in the observed toxicity among the various SSC size fractions may be, in part, explained by their heterogeneous composition. The smallest (0.07, 0.66, and 1.58 μm) diameter particles modestly reduced cell viability, the 13.5 and 5.0 μm particles elicited little to no cytotoxicity at the observed exposure concentration. One objective of this work was to determine if the larger particles delivered via aspiration in our previous in vivo study could have contributed to the observed toxicity. Based on these findings, the larger particles appear to be of lesser toxicity than the respirable and nano-sized fractions.

Another important factor in SSC particle-induced toxicity is its unique chemical composition. While there are apparently no other studies of the cellular toxicity of SSC, there have been some investigations of its constituent components, namely ATH and

polymethylmethacrylate (PMMA). ATH is an insoluble chemical intermediate to aluminum oxide production produced by the Bayer process and is widely used in the plastics industry as a flame retardant and pigment (Huber Materials, 2013). Immune cell reactivity to ATH has been characterized in the context of vaccine adjuvant interactions with macrophages. In this application, ATH acts to aggregate antigens and promote their interaction with immune cells (HogenEsch et al., 2018). ATH also enhances the uptake of antigens by antigen-presenting cells and activates the NLRP3 inflammation pathway (He et al., 2015). Supporting our findings of increased levels of IL-1β in response to SSC, ATH activates aspartate proteases through NLRP3, leading to the modification of *pro*-caspase-1 and IL-1β in normal human peripheral blood - mononuclear cells (Li et al., 2007) and bone-marrow-derived macrophages (Franchi and Núñez, 2008). ATH adjuvant exposure of 11 μg/ml resulted in 50% macrophage mortality (Rimaniol et al., 2004). ATH in a 1 mg/ml suspension induced an approximately three-fold increase in LDH release in both cultured macrophages and PMNs (Goto et al., 1993). Disruption of lysosomes and ROS production after ATH phagocytosis were also noted (Li et al., 2007). PMMA, often a component of surgical implants (Horowitz and Purdon, 1995), is capable of releasing particles as the material degrades. Exposure to 0.325 μm diameter PMMA particles induced the release of arachidonic acid products, LDH, impairment of cellular function, and eventual cell disintegration in cultured P388D1 macrophages. Human primary blood monocytes released inflammatory cytokines, prostaglandin E_2, and hexosaminidase in response to exposure to 0.325 μm diameter PMMA particles, although significant reductions in viability were not detected (Gonzalez et al., 1996). Inhalation exposure to monomeric MMA at 1000 ppm for 6 h/day, 5 days/week, for 4 weeks resulted in airway inflammation, including bronchopneumonia and emphysema, as well as decreased lung glutathione levels in rats (Aydin et al., 2002). There have been no apparent investigations of either ATH or PMMA particles when introduced to the lung or in lung-specific cell culture.

One additional contributor to SSC toxicity is its apparent ability to elicit ROS generation. ROS are the unstable molecules formed as by-products of mitochondrial electron transport or spontaneously by some types of particles (Fubini and Hubbard, 2003). ROS species include superoxide anion radicals, hydroxyl radicals, singlet oxygen, and hydrogen peroxide. ROS play a particularly important role in macrophages, which engulf foreign material into phagolysosomes, where they are subsequently degraded (Kreyling, 1992). While ROS are components of cell signaling and phagocytosis of foreign material under normal physiologic conditions, their overabundance can induce oxidative stress and reduce viability. Particulate-cell interactions have been shown to induce a variety of ROS-mediated damage, including mitochondrial dysfunction (Alshatwi et al., 2013), DNA damage (Nabeshi et al., 2011; Olgun et al., 2017), membrane damage autophagy (Li et al., 2010), apoptosis (Hiura et al., 1999), and genotoxicity (Knaapen et al., 2004). We intend to further investigate this potential mechanism of toxicity in future studies. The GPx-1-PTP1B-PP2A axis is an important system for moderating the ROS generated during inflammatory responses, and GPx-1-PTP1B-PP2A signaling may be reduced in some cases of advanced lung disease (Geraghty et al., 2013). We observed increased GPx activity at 12.5, 25, and 50 μg/ml exposure levels, possibly indicating a compensatory anti-inflammatory response. Increased GPx has been associated with other pulmonary diseases characterized by

inflammation, including chronic beryllium disease (Comhair et al., 1999) and asthma (Smith et al., 1993). The reduction in GPx levels observed at 100 μg/ml is possibly due to the overall reduction in cell viability as observed in Figure 4.

Our study design using one phagocytic cell line examined at one time point may have not provided a complete picture of the ROS response to SSC exposure. It is possible that the ROS we observed was not from early by particle-cell interaction, but rather, a later by-product associated with adjacent cell exposure to ROS and phagolysosomal cytotoxic constituents. Unfortunately, extremely limited quantities of SSC samples precluded more time points and cell lines in this case. Another potential limitation is particle interference with the in vitro assays. Optical interference was tested for each assay, and none observed, but it is possible that the particles may have interfered by inhibiting assay enzyme function, adsorbing dyes or cytokines, or quenching fluorescence as some particles, including metal oxides, have been reported to do (Kroll et al., 2012). However, the variety of different toxicity assays performed in this study suggests that these findings are not an artifact of particle interference. Another important limitation of this study is the lack of exposure of cells to VOCs. We have recently determined that MMA vapor is released during sawing (Kang et al., 2019). These VOCs were not collected or delivered to the cell culture in this case. Different rates of polymer vaporization may also explain the differences in aluminum content for each size fraction (Table 1). Future work should determine the toxicity of these VOCs alone and in combination with particle exposure.

Our group recently reported the in vivo responses of the murine lung to SSC. To make comparisons to the present study, it is helpful to relate exposure concentrations between each study. One measure by which this can be achieved is through comparing particle deposition per mouse alveolar surface area (82.2 cm^2) (Knust et al., 2009) to 96-well plate surface area (0.3 cm^2). In the in vivo study, the exposure levels ranged from 0.76 μg SSC/cm^2 to 12.1 μg SSC/cm^2. In this study, our exposures ranged from 0.95 μg/cm^2 to 60.6 μg/cm^2. These estimates assume that 100% of the material is deposited on the surface of alveoli and well, respectively. In both studies, we observed a pattern of cytokines indicative of a mixed Th1 and Th2 cytokine response. In the mouse exposures, TH1 cytokines IL-2, IFNγ, and TNFα were elevated at higher exposure levels. In the macrophage supernatant, IFNγ and TNFα were increased at the 6.25 μg/ml level and above. Th2 cytokines IL-10, IL-4, and IL-5 were elevated at day 1 at all exposure levels in mice, while the same was true for IL-4 in this study. IL-13 was only elevated at 25 and 100 μg/ml exposure levels. IL-6, which is more commonly associated with lung epithelial cell inflammation (Carter et al., 1997), was not elevated in the macrophage supernatant at any level. Increased levels of IL-1β in both studies indicate the activation of the NLR3P inflammasome (Borthwick, 2016; Franchi and Núñez, 2008; He et al., 2016). In mouse BALF, LDH was elevated at all levels at the 24-h time point. In comparison, in THP-1 culture, LDH was only elevated in the 25 μg/mL and higher exposure levels. While comparisons between the two exposure models are limited due to SSC particle population and the single cell line used in this study, these findings indicate that some of the LDH detected in the BALF at lower exposure levels came from cell types other than macrophages.

Conclusions

The present study provides evidence that respirable-sized SSC sawing particles are cytotoxic at a range of exposure concentrations and particle sizes, and they support our earlier in vivo work. SSC particles were observed in phagolysosomes, while others appeared not to be enveloped by a membrane, suggesting that SSC particles are capable of crossing the plasma membrane and entering the cytoplasm. We demonstrated that exposure to respirable particles from SSC sawing induces dose-dependent toxicity in cultured THP-1 macrophages. SSC particles induced cellular ROS production, GPx activation, and toxic oxidative stress. Furthermore, we observed that in size-selective SSC samples, the smallest (0.07 μm) diameter particles induced greater toxicity per unit mass compared to other size fractions. These results suggest that sawing SSC may pose a respiratory hazard, as particles capable of reaching the deep lung were shown to be cytotoxic. These findings have important occupational relevance and suggest that efforts to mitigate exposure to nano-sized particles emitted during sawing may be necessary. However, further work is necessary to elucidate the mechanisms of toxicity, the role of VOCs emitted during sawing, and to determine the effect of repeated, occupationally relevant exposures to particles generated in real time.

Funding

The author(s) received no financial support for the research, authorship, and/or publication of this article.

References

Alshatwi AA, Subbarayan PV, Ramesh E, et al. (2013) Aluminium oxide nanoparticles induce mitochondrial-mediated oxidative stress and alter the expression of antioxidant enzymes in human mesenchymal stem cells. Food Additives & Contaminants: Part A: Chemistry, Analysis, Control, Exposure & Risk Assessment 30: 1–10.

Aydin O, Attila G, Dogan A, et al. (2002) The effects of methyl methacrylate on nasal cavity, lung, and antioxidant system (an experimental inhalation study). Toxicologic Pathology 30: 350–356. [PubMed: 12051552]

Borthwick LA (2016) The IL-1 cytokine family and its role in inflammation and fibrosis in the lung. Seminars in Immunopathology 38: 517–534. [PubMed: 27001429]

Carter JD, Ghio AJ, Samet JM, et al. (1997) Cytokine production by human airway epithelial cells after exposure to an air pollution particle is metal-dependent. Toxicology and Applied Pharmacology 146: 180–188. [PubMed: 9344885]

Comhair SA, Lewis MJ, Bhathena PR, et al. (1999) Increased glutathione and glutathione peroxidase in lungs of individuals with chronic beryllium disease. American Journal of Respiratory Critical Care Medicine 159: 1824–1829. [PubMed: 10351926]

DuPont (2018) Corian Solid Surface Product Overview. Wilmington: Corian Design.

Franchi L and Núñez G (2008) The NLRP3 inflammasome is critical for aluminium hydroxide-mediated IL-1β secretion but dispensable for adjuvant activity. European Journal of Immunology 38: 2085–2089. [PubMed: 18624356]

Freedonia Inc (2015) Countertops, Industry Study.

Fubini B and Hubbard A (2003) Reactive oxygen species (ROS) and reactive nitrogen species (RNS) generation by silica in inflammation and fibrosis. Free Radical Biology and Medicine 34: 1507–1516. [PubMed: 12788471]

Fugazzi R (1998) Solid Surface Composite and Method of Production. US5976670A. Architectural Precast.

Gannon P and Rickard RW (2014) Pulmonary fibrosis associated with aluminum trihydrate (Corian) dust. New England Journal of Medicine 370: 2156–2157.

Geiser M and Kreyling WG (2010) Deposition and biokinetics of inhaled nanoparticles. Particle and Fibre Toxicology 7: 2–2. [PubMed: 20205860]

Geraghty P, Hardigan AA, Wallace AM, et al. (2013) The glutathione peroxidase 1-protein tyrosine phosphatase 1B-protein phosphatase 2A axis. A key determinant of airway inflammation and alveolar destruction. American Journal of Respiratory Cell and Molecular Biology 49: 721–730. [PubMed: 23590304]

Gonzalez O, Smith RL and Goodman SB (1996) Effect of size, concentration, surface area, and volume of polymethylmethacrylate particles on human macrophages in vitro. Journal of Biomedical Materials Research 30: 463–473. [PubMed: 8847354]

Goto N, Kato H, Maeyama J-I, et al. (1993) Studies on the toxicities of aluminium hydroxide and calcium phosphate as immunological adjuvants for vaccines. Vaccine 11: 914–918. [PubMed: 8212836]

Hardy CL, LeMasurier JS, Mohamud R, et al. (2013) Differential uptake of nanoparticles and microparticles by pulmonary APC subsets induces discrete immunological imprints. Journal of Immunology 191: 5278.

He P, Zou Y and Hu Z (2015) Advances in aluminum hydroxide-based adjuvant research and its mechanism. Human Vaccine Immunotherapy 11: 477–488.

He Y, Hara H and Nunez G (2016) Mechanism and regulation of NLRP3 inflammasome activation. Trends in Biochemical Science 41: 1012–1021.

Hiura TS, Kaszubowski MP, Li N, et al. (1999) Chemicals in diesel exhaust particles generate reactive oxygen radicals and induce apoptosis in macrophages. Journal of Immunology 163: 5582–5591.

HogenEsch H, O'Hagan DT and Fox CB (2018) Optimizing the utilization of aluminum adjuvants in vaccines: you might just get what you want. NPJ Vaccines 3: 51. [PubMed: 30323958]

Horowitz SM and Purdon MA (1995) Mechanisms of cellular recruitment in aseptic loosening of prosthetic joint implants. Calcified Tissue International 57: 301–305. [PubMed: 8673868]

Huber Materials (2013) Alumina Trihydrate (ATH) – A Versatile Pigment for Coatings, Inks, Adhesives, Caulks, Sealants, Potting and Encapsulating Applications. Huber Materials.

Kang S, Liang H, Qian Y, et al. (2019) The composition of emissions from sawing Corian®, a solid surface composite material. Annals of Work Exposure and Health 63: 480–483.

Knaapen AM, Borm PJA, Albrecht C, et al. (2004) Inhaled particles and lung cancer. Part A: mechanisms. International Journal of Cancer 109: 799–809. [PubMed: 15027112]

Knust J, Ochs M, Gundersen HJ, et al. (2009) Stereological estimates of alveolar number and size and capillary length and surface area in mice lungs. The Anatomical Record 292: 113–122. [PubMed: 19115381]

Kreyling WG (1992) Intracellular particle dissolution in alveolar macrophages. Environmental Health Perspectives 97: 121–126. [PubMed: 1396446]

Kroll A, Pillukat MH, Hahn D, et al. (2012) Interference of engineered nanoparticles with in vitro toxicity assays. Archives of Toxicology 86: 1123–1136. [PubMed: 22407301]

Li H, Nookala S and Re F (2007) Aluminum hydroxide adjuvants activate caspase-1 and induce IL-1β and IL-18 release. Journal of Immunology 178: 5271–5276.

Li JJ, Hartono D, Ong C-N, et al. (2010) Autophagy and oxidative stress associated with gold nanoparticles. Bio-materials 31: 5996–6003.

Mandler WK, Qi C, Orandle MS, et al. (2019) Mouse pulmonary response to dust from sawing Corian®, a solid-surface composite material. Journal of Toxicology and Environmental Health, Part A 82(11): 645–663. [PubMed: 31290376]

McKeever R, Okaneku J and LaSala GS (2014) More on pulmonary fibrosis associated with aluminum trihydrate (Corian) dust. New England Journal of Medicine 371: 973.

Nabeshi H, Yoshikawa T, Matsuyama K, et al. (2011) Amorphous nanosilica induce endocytosis-dependent ROS generation and DNA damage in human keratinocytes. Particle and Fibre Toxicology 8: 1. [PubMed: 21235812]

NIOSH (2003) Elements by ICP NIOSH Manual of Analytical Methods. Cincinnati: National Institute of Occupational Safety and Health.

Oberdörster G (2000) Pulmonary effects of inhaled ultrafine particles. International Archives of Occupational Environmental Health 74: 1–8.

Olgun NS, Morris AM, Barber TL, et al. (2017) Comparison of the toxicity of sintered and unsintered indium-tin oxide particles in murine macrophage and epidermal cells. Toxicology and Applied Pharmacology 331: 85–93. [PubMed: 28552777]

Phillips ML and Johnson AC (2012) Prevalence of dry methods in granite countertop fabrication in Oklahoma. Journal of Occupational Environmental Hygiene 9: 437–442. [PubMed: 22650974]

Qi C, Echt A and Murata TK (2016) Characterizing dust from cutting Corian®, a solid-surface composite material, in a laboratory testing system. Annals of Occupational Hygiene 60: 638–642.

Raghu G, Collins BF, Xia D, et al. (2014a) Pulmonary fibrosis associated with aluminum trihydrate (Corian) dust. New England Journal of Medicine 370: 2154–2156.

Raghu G, Xia D and Abraham JL (2014b) More on pulmonary fibrosis associated with aluminum trihydrate (Corian) dust. New England Journal of Medicine 371: 973–974.

Rimaniol A-C, Gras G, Verdier F, et al. (2004) Aluminum hydroxide adjuvant induces macrophage differentiation towards a specialized antigen-presenting cell type. Vaccine 22: 3127–3135. [PubMed: 15297065]

Simmons J (2004) Solid Surface Composites. US20060112646A1.

Smith LJ, Houston M and Anderson S (1993) Increased levels of glutathione in bronchoalveolar lavage fluid from patients with asthma. American Review of Respiratory Disease 147: 1461–1461.

Stanley JK, Coleman JG, Weiss CA, et al. (2010) Sediment toxicity and bioaccumulation of nano and micron-sized aluminum oxide. Environmental Toxicology and Chemistry 29: 422–429. [PubMed: 20821462]

Unwin J, Coldwell MR, Keen C, et al. (2013) Airborne emissions of carcinogens and respiratory sensitizers during thermal processing of plastics. Annals of Occupational Hygiene 57: 399–406.

Wagner AJ, Bleckmann CA, Murdock RC, et al. (2007) Cellular interaction of different forms of aluminum nanoparticles in rat alveolar macrophages. Journal of Physical Chemistry B 111: 7353–7359.

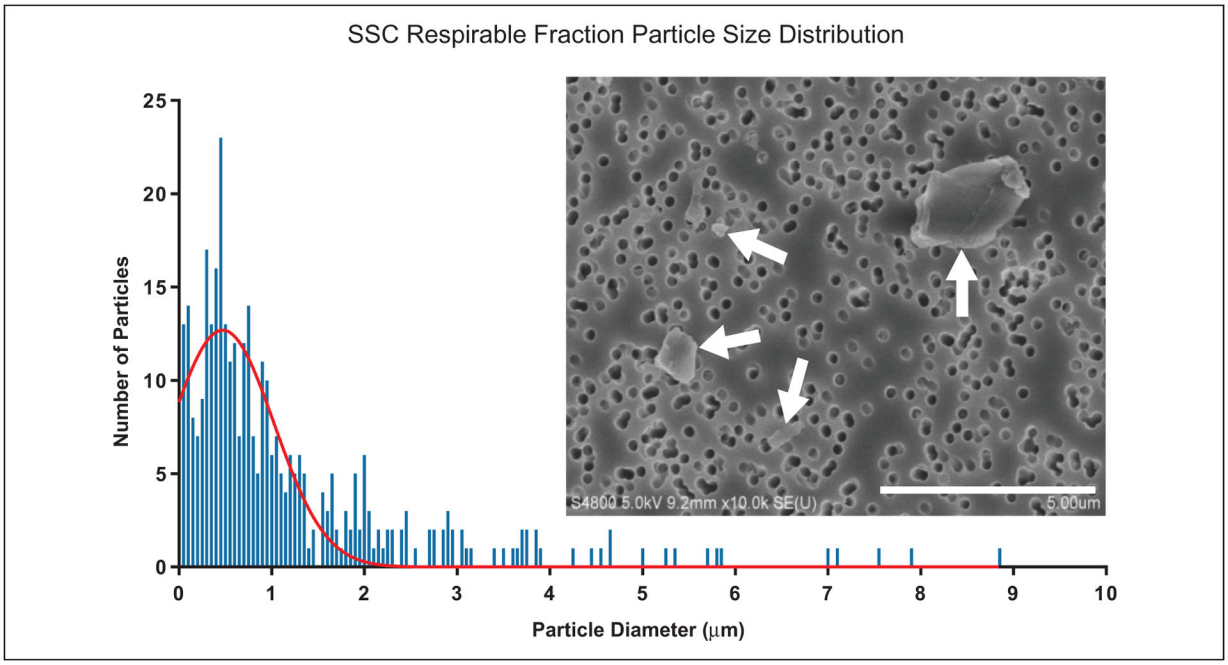

Figure 1.

SSC respirable fraction particle size distribution. The geometric mean particle size was 0.72 μm, with a geometric standard deviation of 2.9. Of the observed particles, 95.6% were smaller than 4 μm in diameter. White arrows indicate SSC particles (inset). SSC: solid surface composite.

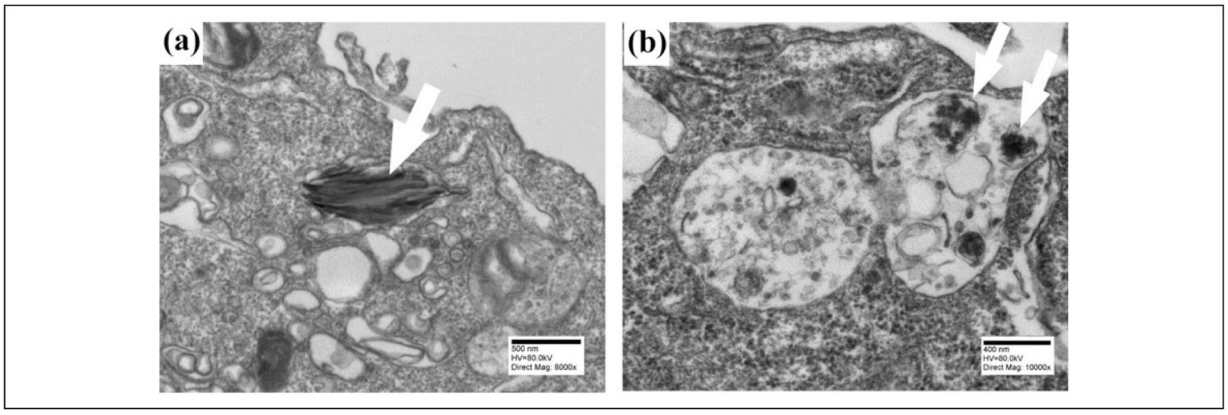

Figure 2.

Localization of respirable SSC particles within THP-1 derived macrophages. Transmission electron micrographs indicate the presence of SSC particles in the cytoplasm (a) and contained within vesicles (b) 24 h postexposure to 100 μg/ml SSC. SSC: solid surface composite.

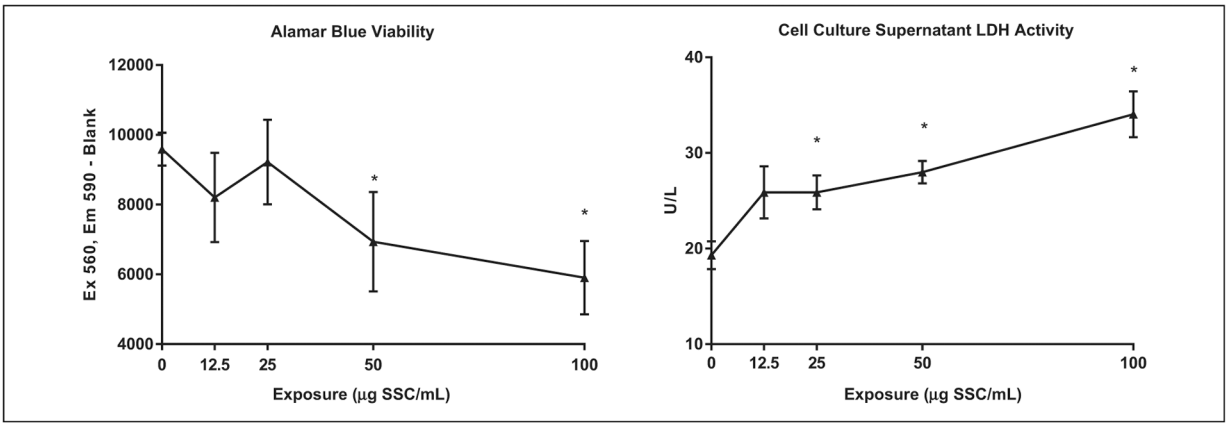

Figure 3.

SSC exposure-induced cytotoxicity. THP-1 derived macrophages exposed to SSC particles exhibit a dose-dependent decrease in viability/metabolic activity as indicated by a decreased rate of resazurin to conversion resorufin (left), and decreased membrane integrity as indicated by increased supernatant LDH activity (right). Values are means ± SEM. * indicates significant difference ($p < 0.05$) compared to control. SSC: solid surface composite; LDH: lactate dehydrogenase.

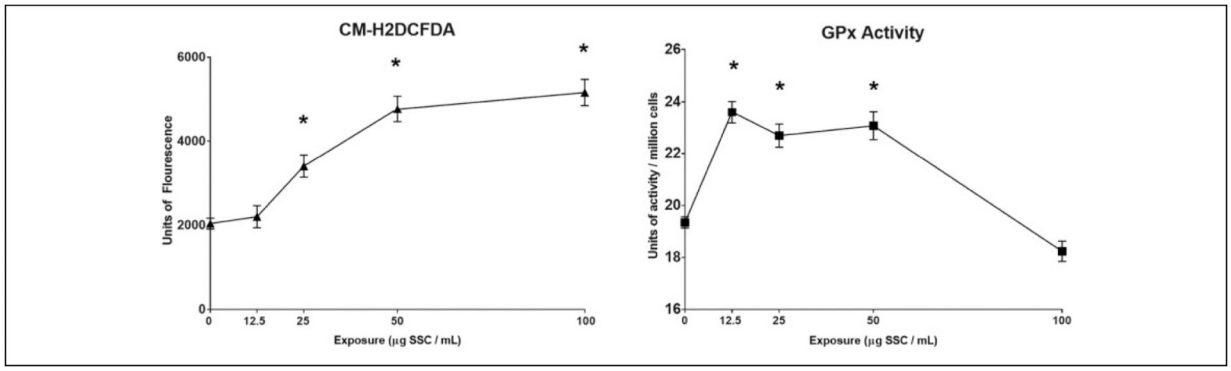

Figure 4.

SSC exposure induces oxidative stress. Increased CM-H_2DCFDA fluorescence in a dose-dependent manner following respirable SSC exposure of THP-1 derived macrophages (left panel), indicating increased oxidative stress. GPx activity was increased at the 12.5, 25, and 50 μg/ml exposure levels, but was not different from control levels at 100 μg/ml exposure (right panel). Values are means ± SEM. * indicates significant difference ($p < 0.05$) compared to control. SSC: solid surface composite; GPx: glutathione peroxidase; CM-H_2DCFDA: chloromethyl dichlorodihydrofluorescein diacetate.

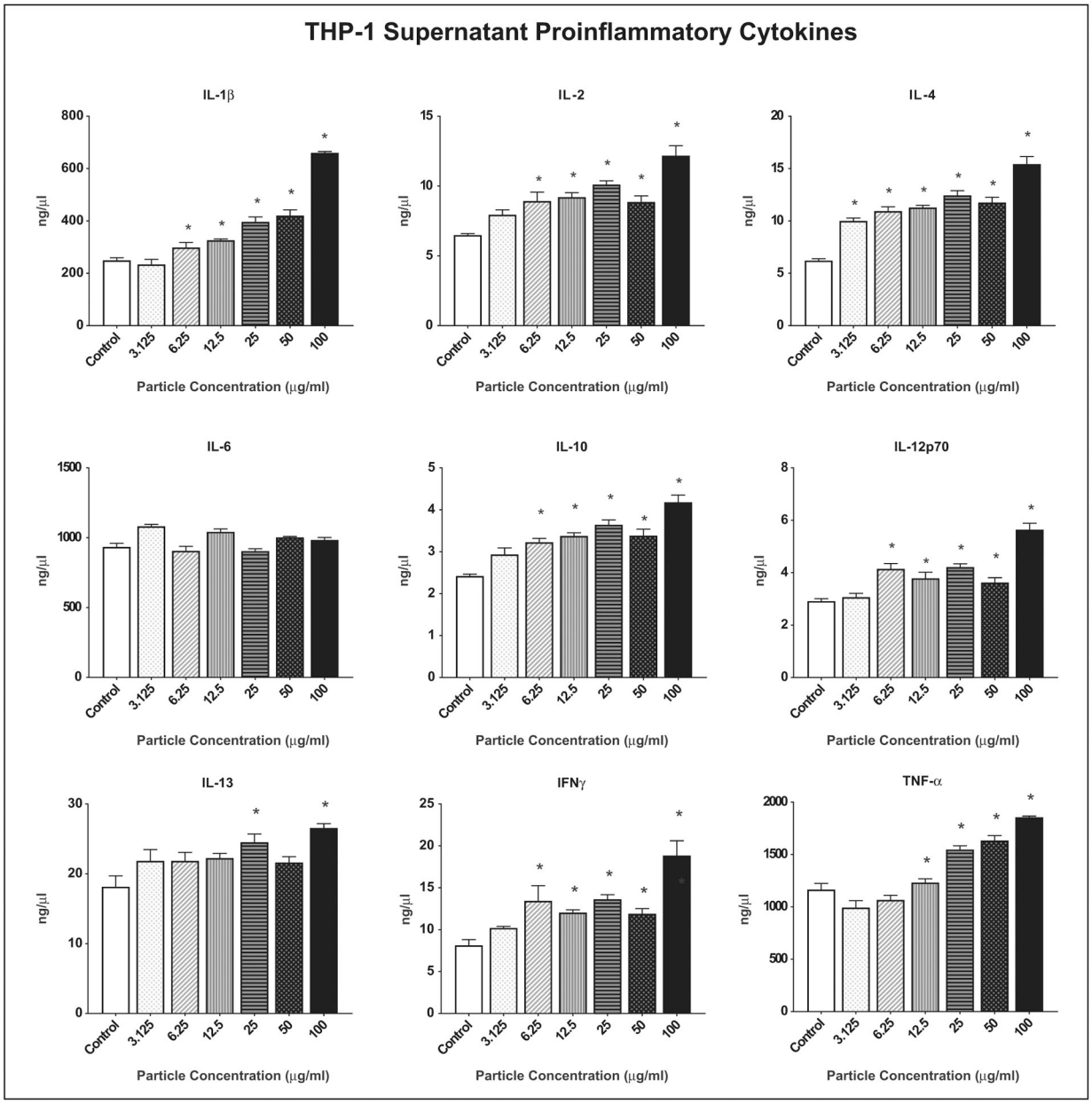

Figure 5.

THP-1 macrophage pro-inflammatory cytokine production in response to SSC. Cytokines were measured via multiplex detection (mesoscale discovery) in the cell culture supernatant of THP-1 derived macrophages exposed to a range of SSC concentrations. Values are means ± SEM. * indicates significant difference ($p < 0.05$) compared to control. SSC: solid surface composite.

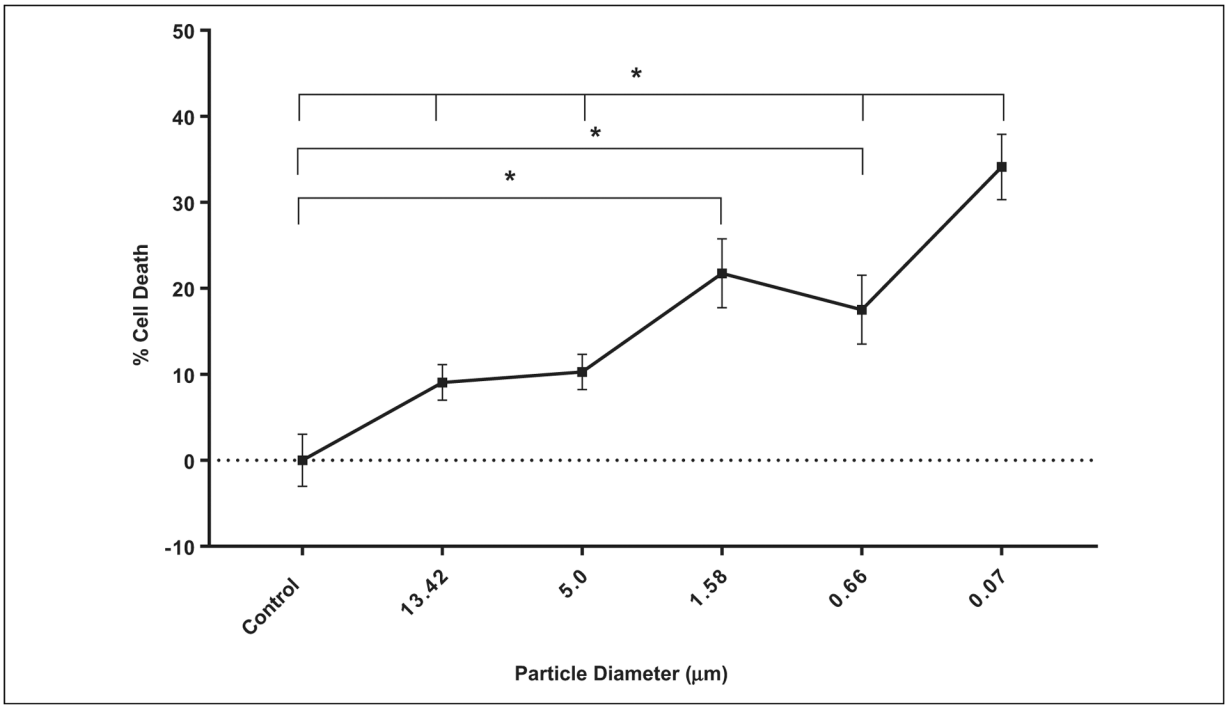

Figure 6.

SSC particle size-fraction cytotoxicity. THP-1 derived macrophage cell culture supernatant LDH activity is increased in a particle size-dependent manner following 24 h exposure to 100 μg/ml for each size fraction. Values are means ± SEM. * indicates significant difference ($p < 0.05$). SSC: solid surface composite; LDH: lactate dehydrogenase.

Table 1.

SSC sawing particle's estimated aluminum content.[a]

Particle diameter (μm)	13.5	5.0	1.58	0.66	0.07
Elemental Al %	19	27	30	37	24
Calculated ATH %	52	74	83	102	66

SSC: solid surface composite; Al: aluminum; ATH: aluminum trihydrate.

[a]Size-fraction samples' Al content was analyzed using inductively coupled plasma - atomic emission spectroscopy according to NIOSH standard 7303. Sample estimated %ATH was calculated based on the ratio of the atomic mass of Al/ATH.